AIP | The Journal of Chemical Physics

Multiple scattering mechanisms causing interference effects in the differential cross sections of H + D2 → HD(v′ = 4, j′) + D at 3.26 eV collision energy

Mahima Sneha, Hong Gao, Richard N. Zare, P. G. Jambrina, M. Menéndez, and F. J. Aoiz

Citation: The Journal of Chemical Physics **145**, 024308 (2016); doi: 10.1063/1.4955294
View online: http://dx.doi.org/10.1063/1.4955294
View Table of Contents: http://scitation.aip.org/content/aip/journal/jcp/145/2?ver=pdfcov
Published by the AIP Publishing

THE JOURNAL OF CHEMICAL PHYSICS **145**, 024308 (2016)

Multiple scattering mechanisms causing interference effects in the differential cross sections of $H + D_2 \rightarrow HD(v' = 4, j') + D$ at 3.26 eV collision energy

Mahima Sneha,[1] Hong Gao,[1,a)] Richard N. Zare,[1,b)] P. G. Jambrina,[2] M. Menéndez,[2] and F. J. Aoiz[2,b)]
[1]*Department of Chemistry, Stanford University, Stanford, California 94305, USA*
[2]*Departamento de Quimica Fisica I, Facultad de Quimica, Universidad Complutense de Madrid, Madrid 28040, Spain*

(Received 29 March 2016; accepted 23 June 2016; published online 13 July 2016)

Differential cross sections (DCSs) for the $H + D_2 \rightarrow HD(v' = 4, j') + D$ reaction at 3.26 eV collision energy have been measured using the photoloc technique, and the results have been compared with those from quantum and quasiclassical scattering calculations. The quantum mechanical DCSs are in good overall agreement with the experimental measurements. In common with previous results at 1.97 eV, clear interference patterns which appear as fingerlike structures have been found at 3.26 eV but in this case for vibrational states as high as $v' = 4$. The oscillatory structure is prominent for low rotational states and progressively disappears as j' increases. A detailed analysis, similar to that carried out at 1.97 eV, shows that the origin of these structures could be traced to interferences between well defined classical mechanisms. In addition, at this energy, we do not observe the anomalous positive j'–θ trend found for the $v' = 4$ manifold at lower collision energies, thus reinforcing our explanation that the anomalous distribution for $HD(v' = 4, j')$ at 1.97 eV only takes place for those states associated with low product recoil energies. *Published by AIP Publishing.* [http://dx.doi.org/10.1063/1.4955294]

I. INTRODUCTION

Differential cross sections (DCSs) are considered to be one of the most sensitive probes of scattering dynamics. It is well known that reactions dominated by collinear approach geometries show preferential backscattering of the products with respect to the direction of approach of the reagents in the center of mass frame, whereas reactions that proceed through a long-lived complex show nearly symmetric forward and backward scattered products.[1,2] During the last two decades, a detailed and insightful picture of the scattering dynamics for the $H + D_2$ bimolecular exchange reaction has emerged through the close collaboration of experiments and theory.[3,4] Of particular interest has been the observation of a fingerlike structure in the DCSs for $HD(v' = 1, j')$ products formed at $E_{coll} = 1.97$ eV.[5,6] These have been established to arise from quantum interferences between different reaction mechanisms that are only present at high enough recoil energies. In this paper, we extend these studies to $HD(v' = 4, j')$ products at a higher collision energy of 3.26 eV. We find that both quantum mechanical (QM) and experimental DCSs for $HD(v' = 4, j' = 3, 5, 6)$ show multiple peaks in the backward/sideways scattered regions. Moreover, the oscillations become less pronounced as product rotation increases. Using a semiclassical analysis, we are able to identify the different reaction mechanisms that participate in causing products in the same internal state to be scattered into the same solid angle element. However, it is only through a fully quantum treatment that we are able to make these identifications. For higher rotational states, some of those mechanisms and their associated interferences disappear, and the oscillatory structures become progressively smoother and finally vanish. In essence, the $H + D_2$ reaction system acts as a multiple slit interferometer.

In contrast to the present work, our previous study of the DCSs for the $H + D_2 \rightarrow HD(v' = 4, j') + D$ reaction at 1.97 eV showed one broad peak and a seemingly anomalous scattering behavior, i.e., the products became more backward scattered as j' increased.[7] Using detailed quasiclassical (QCT) and quantum mechanical (QM) analysis, we attributed this anomaly to the low recoil energy of the products and hence predicted that in the limit of low recoil, the presence of a centrifugal barrier in the exit channel of the reaction diminishes the contribution of high impact parameter collisions, which is responsible for the anomalous behavior of the DCS.[4,7,8] If this argument is indeed true, that anomalous behavior would not be present on DCSs measured at large enough collision energies for the same rovibrational states. As we show in what follows, the product states do follow a negative j'–θ trend, which is expected when the recoil energy is in large excess of the centrifugal barrier. This study presents experimental measurements for the $H + D_2 \rightarrow HD(v' = 4, j') + D$ reaction at the highest collision energy yet studied and compares them to fully quantum and semiclassical calculations.

a)Current address: Department of Chemistry, University of Basel, Klingelbergstrasse 80, CH-4056 Basel, Switzerland.
b)Authors to whom correspondence should be addressed. Electronic addresses: zare@stanford.edu and aoiz@quim.ucm.es

II. EXPERIMENTAL AND THEORETICAL METHODS

A. Experiment

A detailed description of the three-dimensional ion imaging setup[9] and the photoloc[10] used in this study is given elsewhere, and only the important details are described here. A mixture of HBr (~5%) in D_2 (Cambridge Isotope Laboratories, Inc., 99.6% D_2 + 0.4% HD) is supersonically co-expanded into a vacuum chamber using a pulsed general valve (General Valve Series 9) which operates at the repetition rate of 10 Hz and a typical stagnation pressure of about 22 psi. The supersonic expansion internally cools the D_2 molecules to ($v = 0$, $j = 0$, 1, 2) states with a relative population of 0.39:0.31:0.29, respectively. The skimmed molecular beam (2 mm skimmer, Beam Dynamics) is then perpendicularly intersected with two counterpropagating focused laser beams in the extraction region of the Wiley-McLaren time-of-flight mass spectrometer. The reaction is initiated by photodissociating HBr using a focused (through a CaF_2 spherical plano-convex lens with f = 42 cm) vacuum ultraviolet (VUV) laser beam from the fluorine excimer laser (Coherent, ExciStar-XS) which generates translationally hot H atoms with two different collision energies: E_{coll} = 3.26 eV associated with formation of H + Br($^2P_{3/2}$) and E_{coll} = 2.90 eV associated with formation of H + Br($^2P_{1/2}$), referred to as fast and slow channels, respectively. These two channels have the respective ratio of 0.84:0.16 as measured previously.[11]

Both fast and slow H atoms then react with D_2 to form HD(v', j') products. After a delay of 15-20 ns, the HD products are state selectively ionized by a counterpropagating focused UV beam via resonance-enhanced multiphoton ionization (REMPI) on the Q-branch of the (0,4) band of the $E, F^1\Sigma_g^+$–$X^1\Sigma_g^+$ transition. The UV beam is obtained by frequency doubling the output of a dye laser (Lambda physic, LPD 3000) pumped by the third harmonic of an Nd:YAG^{3+} (Quanta-Ray, DCR-3) using a β-barium borate (BBO) crystal. The wavelength of the UV beam is scanned back and forth to cover the whole Doppler profile of the HD products. The HD ions are collected on a position-sensitive multichannel plate detector. The lab frame speed of the HD ions thus measured by the three-dimensional ion imaging setup is converted to a DCS based on the photoloc technique using the fast channel center of mass speed and speed of HD in the center of mass frame.

There are several difficulties associated with using a fluorine excimer laser as photolysis source which are described in detail in our previous publication.[11] In addition to the difficulties mentioned previously, the poor Franck-Condon vibrational overlap[12] lowers the probing efficiency significantly for measuring the DCSs for HD($v' = 4$, j') reported here, further reducing the signal-to-noise ratio. An additional difficulty with the $v' = 4$ manifold is that there is a very strong H^+ signal at most of the [2 + 1] REMPI wavelengths. This signal saturates the detector thus lowering its efficiency for measuring the HD^+ signal. For some j' states, the H^+ signal is so large that the poor signal-to-noise ratio made it impossible to collect any data.

1. Conversion of lab frame speeds to COM angular distributions

As mentioned above, our experiments measure the lab frame speed of the HD products. Using photoloc, the lab frame speed distributions are converted into the center of mass (COM) frame angular distribution by using law of cosines, as shown by the equation

$$\cos\theta = \frac{|v_{HD}|^2 - |u_{com}|^2 - |u_{HD}|^2}{2\,|u_{HD}|\,|u_{com}|}, \tag{1}$$

where u_{com} and u_{HD} are the center of mass speed and the speed of HD in the center of mass frame. Both are fixed by the energetics of the reaction, thus providing a one-to-one mapping between lab frame HD speed and θ,

$$|u_{com}| = \frac{m_H}{m_H + m_{D_2}}\sqrt{\frac{2E_H}{m_H}}, \tag{2}$$

$$E_H = \frac{m_X\,(h\nu - D_0\,(HBr))}{m_X + m_H}, \tag{3}$$

$$|u_{HD}| = \frac{m_D}{m_{HD} + m_D}\sqrt{\frac{2\left(E_{int} + E_{coll} - E'_{int} - \Delta D_0\right)}{\mu'}}, \tag{4}$$

$$E_{coll} = \frac{\mu E_H}{m_H}, \tag{5}$$

where $h\nu$ is the photolysis laser energy (7.87 eV), μ is the reduced mass of reactants, and μ' is the reduced mass of products; D_0(HBr) (3.75 eV) is the dissociation energy of HBr and ΔD_0 is the difference between the dissociation energy of D_2 and HD (0.04 eV). Because D_0(HBr) is different for fast and slow channels, it is evident that the fast and slow channels will have different values of u_{com} and u_{HD}. Because the experimental speed distribution is a combination of both slow and fast channels, a conversion of the experimental lab frame speeds into angles becomes inaccurate. A more accurate representation, therefore, would be to plot the speed distributions for both experiment and theory and compare the respective results. Although for comparison purposes it may be a good approach, however, DCS is considered to be a universal probe of reaction dynamics. Hence, if we still wish to use the DCS, does converting speeds into angles using fast channel photoloc parameters still work? There are two ways this can work: (i) if the slow channel contribution is relatively small, it should not affect the final result. However, we have shown in our previous publication that this is not the case.[11] Although the slow channel contribution is only 16%, because of the high cross sections at 2.90 eV for the HD product states reported here, its contribution cannot be neglected (see Figure 1(a)). (ii) If u_{HD} and u_{com} for slow and fast channels are analogous, their conversion to θ values should be similar. Figure 1(b) shows the one-to-one mapping between the angles and lab frame speeds for HD($v' = 4$, $j' = 3$) for both fast and slow channels. It is evident that in the regions where most of the product angular distribution is prominent, i.e., between 80° and 150°, the curves for slow and fast channel only differ by less than 500 m/s. Hence, converting speeds to angles using only fast channel parameters does not introduce much inaccuracies and allows us to plot our data in the form of DCSs.

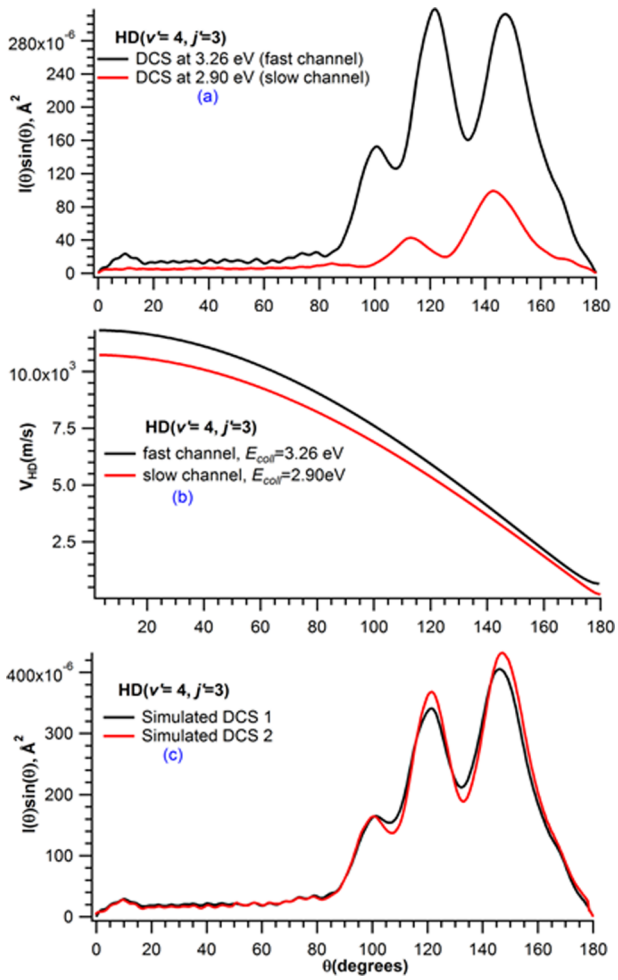

FIG. 1. Data for HD($v'=4$, $j'=3$) showing (a) quantum mechanical DCSs for the slow channel and fast channel multiplied by their relative ratio (0.84:0.16 for fast:slow), (b) plots for one-to-one mapping between lab frame HD speed (v_{HD}) and θ for the fast channel and slow channel speeds at $E_{coll} = 3.26$ eV and 2.90 eV, respectively, and (c) QM DCSs comparing two blurring procedures: the black curve represents DCS obtained by adding the slow and fast channel DCSs in their respective branching ratio. The red curve represents DCS obtained by converting DCSs at $E_{coll} = 3.26$ eV and 2.90 eV to their respective speed distributions. The speed distributions are then added in their respective branching ratio and converted back to DCS using fast channel photoloc parameters. As can be seen, there is not much difference between the two DCSs.

B. Time-independent quantum mechanical (TI-QM) calculations

Time-independent quantum mechanics (TI-QM) calculations were carried out on the BKMP2[13] potential energy surface (PES) using the coupled-channel hyperspherical method implemented in the ABC code.[14] To simulate the experimental conditions accurately, two sets of TI-QM calculations were carried out. To account for the slow channel, calculations were carried out at total energies of about $E_{tot} = 3.10$ eV (which for $D_2(v = 0, j = 0)$ corresponds to $E_{coll} = 2.90$ eV). A second batch was performed at 23 collision energies, in the 3.14–3.35 eV range for $j = 0$, and similarly for $j = 1$ and 2, to simulate the fast channel. The propagation was performed in 250 sectors from 0.8 to 24 a_0, including in the basis all the diatomic energy levels up to 4.50 eV and helicity quantum numbers up to $\Omega_{max} = 15$. All the partial waves up to $J = 50$ were included.

1. Quasiclassical trajectories

A batch of 25×10^6 trajectories was run at $E_{coll} = 3.26$ eV for the $H + D_2(v = 0, j = 0)$ on the BKMP2 PES, following the procedures described in a previous publication.[15] An integration step of 0.05 fs and a maximum impact parameter $b = 1.3$ Å (corresponding to $J = 46$) were used in the calculations. The rovibrational energies of the HD product molecules were calculated by semiclassical quantization of the action and their values were fitted to Dunham expansions in $(v' + 1/2)$ and $j'(j' + 1)$. The (real) j' value was assigned by equating the square of the classical HD rotational angular momentum to $j'(j' + 1)\hbar^2$. The value of v' was then obtained by equating the internal energy to a rovibrational Dunham expansion for a specific j' value.

III. RESULTS AND DISCUSSION

Figure 2 shows the experimentally derived (blue dots) and QM (black curves) DCSs for the HD($v' = 4$, j') product states. The theoretical calculations have been averaged over the initial rotational states and experimental collision energy spread. In our experiments, we measure lab frame speed distribution which is then converted into DCS via law of cosines using the photoloc parameters for the fast channel. Experimental speed distribution is a combination of the slow and fast channels (*vide supra*); i.e., the HD products arise from two different groups of collision energies centered at $E_{coll} = 3.26$ eV and 2.90 eV. Hence, to compare theory against experiment, the respective contributions of both the slow ($E_{coll} = 2.90$ eV) and fast ($E_{coll} = 3.26$ eV) channels resulting from the two spin-orbit states of the Br atom formed in the photodissociation have to be included in the simulation. The process, however, is not straightforward[11] and it is summarized below.

The DCSs from both slow and fast channels are individually blurred: (i) each curve is smoothed with a Gaussian to simulate a 0.05 eV spread in experimental collision energies resulting from imperfect translational cooling; (ii) each curve is averaged to account for the D_2 distribution of rotational states (0.39:0.31:0.29 for $j = 0$, 1, and 2, respectively). If we are to follow the correct procedure, the blurred DCSs for each channel should be converted into speed distribution using the photoloc parameters and added together after being weighted by their branching ratio [0.84(fast):0.16(slow)]. The resulting speed distribution should then be converted back into DCS using photoloc parameters for the fast channel, resulting in a theoretical DCS which should simulate the experimental conditions. However, we find that because of the relatively small contribution of the slow channel, the overall theoretical DCS obtained through this rigorous method is similar to that obtained just by adding the convoluted DCS for the slow and fast channel, see Fig. 1(c). Therefore, for the purpose of comparing theory with experiment, we have used the latter procedure. The experimentally derived DCSs, obtained in arbitrary units, have been scaled to fit the simulated DCSs.

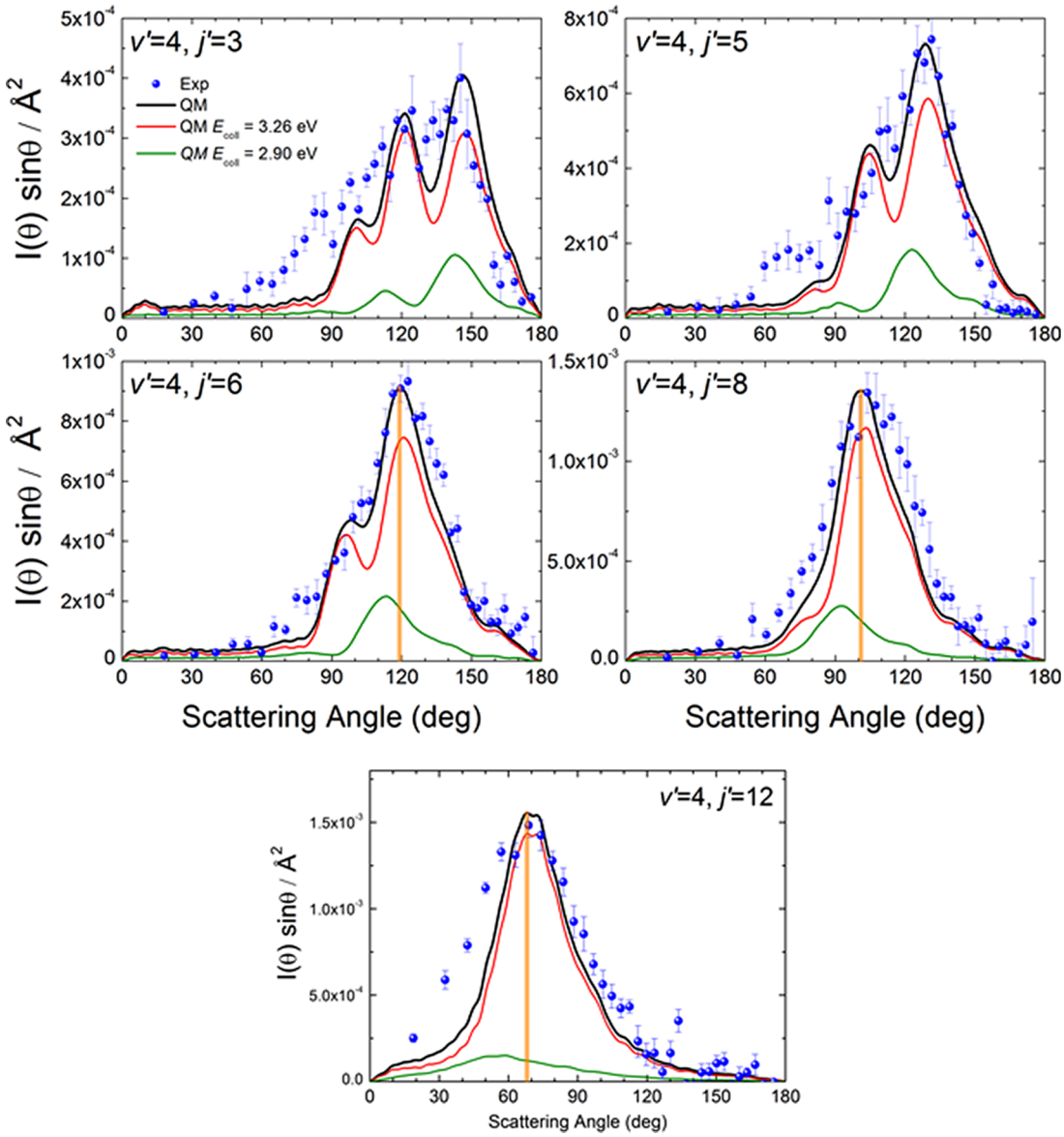

FIG. 2. Comparison of the experimentally derived results (blue points with error bars) with the theoretical DCSs convoluted with the experimental conditions (black line). The error bars represent one standard deviation calculated from the statistical uncertainties in 5-10 different scans. The orange vertical lines drawn in the case of HD($v' = 4$, $j' = 6$, 8, and 12) highlight the peak positions for each of these states, to show the overall forward shift as the j' increases. The decomposition of the theoretical DCSs into the contributions of the fast (red line) and slow (green line) channels is also shown. Although the presence of the slow channel smooths out the total DCS to some extent, it does not suppress the oscillatory structures for $j' = 3$-6. Conversely, it is clear that the observed pattern is not caused by the accidental superposition of the contributions from the slow and fast channels.

There is a general good agreement between experiment and theory, especially at backscattered angles. However, there is a disagreement in the forward hemisphere, and for $j' = 5$ and 6, the second peak (90°-100°) is underestimated by the experiment. The agreement is somewhat better at high rotational states, and for HD($v' = 4$, $j' = 6$, 8), calculations are able to describe the amplitude of the signal between 60°and 90°. This discrepancy was also observed in experiments carried out at lower energies,[16] and the origin of this discrepancy is presently unclear. The second apparent feature is the successive oscillations in the backward hemisphere of the DCSs for low j' values. Although not fully resolved in the experimental data, QM calculations show three main peaks for the DCS of $j' = 3$, two peaks for $j' = 5$ and 6, whereas the DCSs of $j' = 8$ and 12 show only one peak each.

A. Oscillatory pattern in the DCSs and multiple reaction pathways

The presence of several peaks in the angular distributions of the low rotational states of $v' = 4$ resembles those found in the experimental DCSs for HD($v' = 1$, $j' = 0$-4) measured at $E_{coll} = 1.97$ eV, where broad oscillations in the backward hemisphere were interpreted to be the result of interferences between well-characterized mechanisms. However, at $E_{coll} = 1.97$ eV, a single backward peak was observed for the $v' = 4$ manifold, and only one mechanism persists for most of the j' states.

To rule out the possibility that these peaks originated from the sum of the slow and fast channel contributions with maxima at different scattering angles, the decomposition of

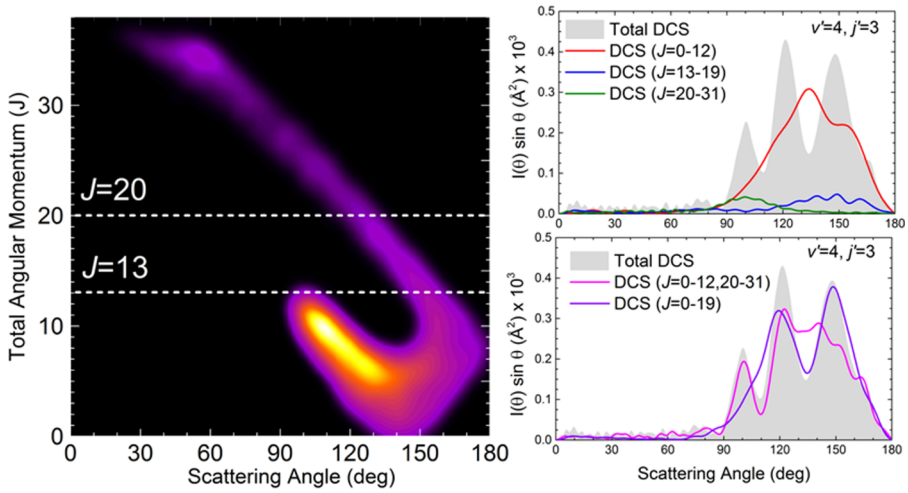

FIG. 3. Origin of multiple peaks in the DCSs of HD($v'=4$, $j'=3$) products. Left panel shows the quasiclassical deflection function while the right panels show the decomposition of the QM angular distributions from the contributions of various sets of J for the same final state. The notation DCS(J_1–J_2) means that the DCS is constructed by including partial waves in the range [J_1, J_2] and the corresponding cross terms.

the theoretically simulated total DCS (black line) into the contributions of the fast (E_{coll} = 3.26 eV, red line) and slow (E_{coll} = 2.90 eV, green line) channels is shown in Fig. 2 along with the experimental data. For both channels, the theoretically simulated DCSs include the averaging over the collision energy spread and initial rotational states. From the depicted results, it is apparent that the oscillatory pattern in the total DCS is mainly from the E_{coll} = 3.26 eV channel. The effect of the contribution from the slow channel is that of smoothing out the various peaks because the maxima and minima in its DCSs are out-of-phase with respect to those found in the fast channel DCSs. Fortunately, its contribution is small enough so that these peaks survive summation of the two channels. Therefore, to elucidate the origin of these peaks, we will restrict our analysis to the DCSs proceeding from the contribution at E_{coll} = 3.26 eV. Moreover, the theoretical analysis will be restricted to the DCS resulting from the reaction with D_2 in $j = 0$. As it was previously shown,[6] the oscillatory pattern becomes smoother with increasing j arising from the incoherent summation of the contributions from different values of the helicity quantum number Ω, the projection of the total angular momentum on the reactant's approach direction.

To analyze the origin of these peaks, we have calculated the classical deflection functions, that is, the joint probability distribution as a function of θ and the total angular momentum J, $D_r(J,\theta) = (2J+1)P_r(J,\theta)\sin\theta$, as shown in the left panels of Figs. 3 and 4. The analysis based on the classical deflection function was previously employed in the case of HD($v'=1$, j') at 1.97 eV to elucidate the origin of multiple peaks in the product DCSs.[5,6] As discussed in previous works, this function provides information on the correlation between total angular momenta (or impact parameters) and the resulting scattering angle. Although the correlation is never one-to-one, for many direct reactions there is a strong correlation between these magnitudes that appears as approximately a broad stripe that moves from low J and angles close to 180° to high J values and small scattering angles in the forward region. Quasiclassical reaction mechanisms are characterized by well-defined ranges of total angular momentum which give rise to scattering at certain angles for a given final rovibrational state. Therefore, the close examination of the deflection functions gives valuable information about the possible, concurrent mechanisms that govern the reactions, their respective weights, and preferences for certain ranges of scattering angles. Moreover, quantum mechanical interferences are expected whenever two distinct mechanisms lead to products scattered into the same solid angle.

Specifically, the deflection function for H + D_2($v = 0$, $j = 0$) → HD($v' = 4$, $j' = 3$) + D, shown in Fig. 3, bears a close resemblance with those found for $v' = 1$ and low j' at 1.97 eV. Roughly speaking, its shape reveals the presence of three different mechanisms. The first is characterized by a band along the main diagonal that runs from low J values and high θ to high J values and scattering angles in the forward region. This mechanism was termed the "*spiral*" in the previous literature,[17] and, as mentioned above, it is the mechanism that can be expected for direct bimolecular reactions, especially in those cases in which the PES is collinearly dominated. The second feature in the $D_r(J,\theta)$ is the short band parallel to the spiral but limited to small J values and scattering in the 90°-140°. By far, the underlying mechanism, which was termed the "*ear*,"[17] accounts for most of the reactivity at this collision energy. This mechanism, for which the transition state tends to be T-shaped, only takes place at sufficiently high collision energies. Finally, the third mechanism, called the "*farside*," connects the other two, ranging from low total angular momenta and scattering angles of about 140° to relatively higher J values (J = 8-10) and extreme backward angles. Trajectories corresponding to this mechanism represent farside scattering with negative deflection angles, in which the orbital angular momentum changes signs after the collision.[17] Simplified cartoons of these mechanisms can be found in Fig. 3 of Ref. 5.

To investigate the origin of the various peaks observed in the angular distributions and their relation with interferences, the QM DCSs can be dissected in the separate contributions of different ranges of J. The right panel of Fig. 3 displays such analysis for the HD($v' = 4$, $j' = 3$) DCS. Rigorously speaking, the quantum analogue to $D_r(J,\theta)$ does not exist because the QM angular distribution requires the coherent sum of elements of the S matrix with different J values, and hence cross terms in the expansion in partial waves.

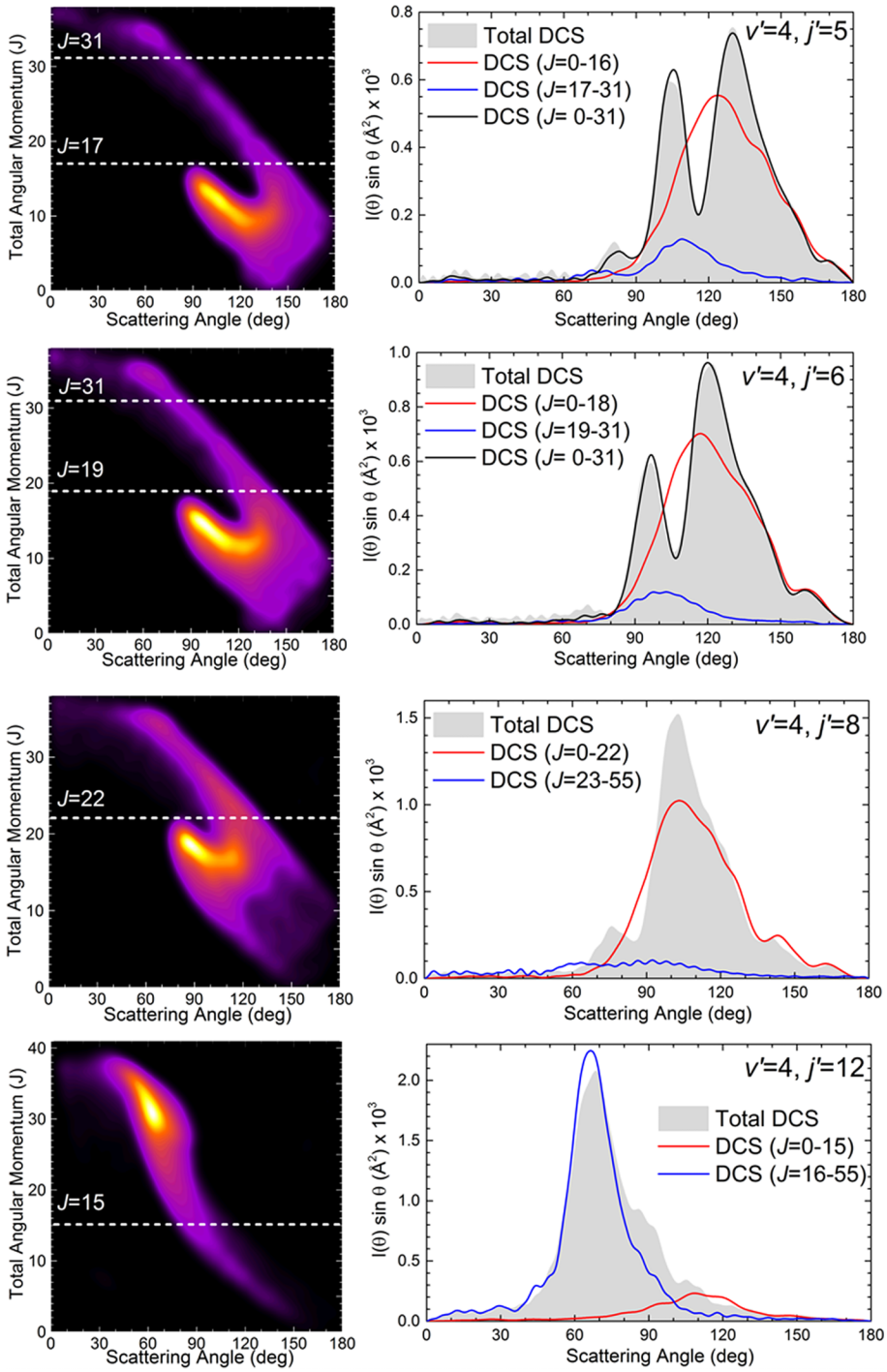

FIG. 4. Same as Fig. 3 but for $j' = 5$, 6, 8, and 12.

Nevertheless, quantum mechanically one can calculate the DCS for a given range of J values, which can be compared to the different regions of classical deflection function. Thus, each of the lines drawn in the right panels of Fig. 3 and labelled as DCS(J_1–J_2) represents the DCS (multiplied by $\sin\theta$), including the contributions of all partial waves in the [J_1, J_2] interval. The gray shaded curve labeled total DCS is calculated by including all partial waves until convergence is achieved. As it is apparent, even though most of the reactivity comes from the *ear* mechanism, the DCS for $J \leq 12$ features only one single peak that does not correspond with any of the three peaks displayed on the global DCS. However, the addition of the J values pertaining to the *spiral*, [J = 13-31], whose separate contribution to the global DCS is minor, dramatically changes the shape of the DCS. Moreover, the various peaks can be traced to interferences between pairs of mechanisms. As it can be inspected in the bottom-right panel of Fig. 3, the peak at $\theta \approx 100°$ is formed by interferences between the *ear* and the partial waves with $J > 19$ belonging to the *spiral*, while the backward peak centered at $\theta \approx 150°$ is formed by interferences between the *farside* and partial waves with $J \leq 19$ belonging to the early part of the *spiral*. In spite of constituting a classical approximation, the predictive power of the QCT deflection function is remarkable. Although the QCT DCS could not account for the several peaks which arise because of the quantum interferences, the $D_r(J,\theta)$ serves to

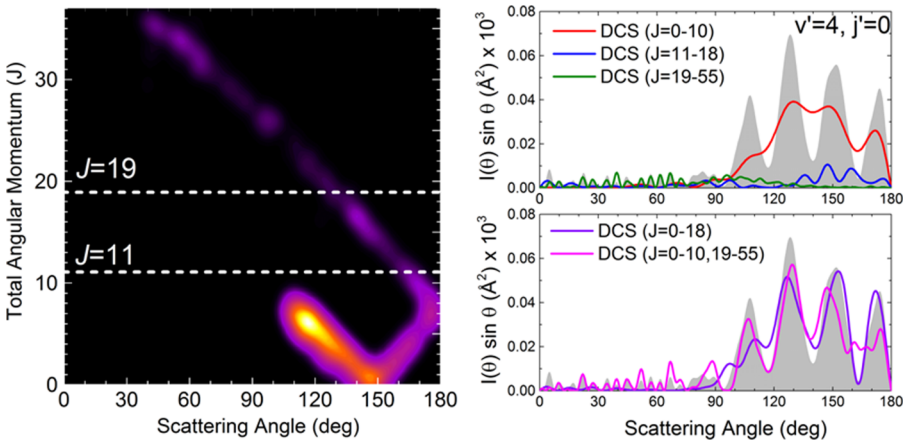

FIG. 5. Same as Fig. 3 but for $j' = 0$.

elucidate which mechanisms, and which groups of partial waves, contribute to each mechanism and when interferences are expected to govern the angular distribution.[5]

Similarly to what was observed for HD($v' = 1$, j') at $E_{coll} = 1.97$ eV, the individual mechanisms lose their identity with increasing j', leading to the progressive smoothing out of the fingerlike structures. The general trend is the merging of the *ear* with the *spiral* and the disappearance of the *farside*. For $j' = 5$ and 6, the DCSs show only two backward peaks that are once more formed by the interference between the *spiral* and the *ear* (top panels Fig. 4). For $j' = 8$, the *ear* and the *spiral* have been almost coalesced in $D_r(J,\theta)$, causing the second peak in the total DCS to almost vanish, surviving as a small shoulder. For $j' = 12$, it is not possible to separate the two mechanisms, and the DCS shows a single peak shifted toward the forward hemisphere. For completeness, we plot the contributions of low J and high J values to the QM DCS and, contrary to what was observed for lower j' states, it leads to almost additive DCSs. In the absence of two different mechanisms, the interferences have disappeared.

It is quite apparent that interferences are more evident for low j' states. Although because of the experimental difficulties mentioned above, it was not possible to measure the angular distributions for HD($v' = 4$, $j' = 0$), it is worthwhile to analyze the theoretical DCS for this state at $E_{coll} = 3.26$ eV. As can be seen in Fig. 5, the separation between the *ear* and the *spiral* in the $D_r(J,\theta)$ is more noticeable and gives rise to four distinct, sharp peaks in the angular distribution. As can be predicted from the deflection function, interferences between partial waves pertaining to the *ear*, the *farside*, and low J values of the *spiral* bring forth the two most backward peaks. Similarly, the peaks at $\theta \approx 105°$ and $\theta \approx 125°$ appear when interferences between the partial waves of the *ear* and the high J parts of the *spiral* are considered.

From the above discussion and the results shown in Figs. 3-5, it is evident that the existence of interferences requires the presence of the *ear* mechanism, which is the most dominant one in the $v' = 4$ manifold for low j' states. In comparison at $E_{coll} = 1.97$ eV, direct recoil or the *spiral* mechanism is the only mechanism present for most of the $v' = 3$, 4 states, except in the case of HD($v' = 3$, $j' = 0$, 1) and HD($v' = 4$, $j' = 1$) where a time-delayed mechanism[18] gives rise to the peak in the extreme forward region. This behavior does not seem so surprising if we consider the relationship between different mechanisms involved and the total energy available to the reaction. At 1.97 eV, most of the available energy is tied up into the internal energy of the products for the $v' = 3$ and 4 product states. Hence, the only mechanism that leads to any products is the one that follows the minimum energy path. However, at $E_{coll} = 3.26$ eV, there is enough energy available to the system to form products in the $v' = 4$ manifold through other pathways, such as the *ear* in which the T-shaped transition state offers a higher barrier. If the energy requirement for the reaction to follow this pathway is fulfilled, the higher cone of acceptance makes it more probable compared to the *spiral* mechanism, which takes place through a collinear transition state. In the case of HD($v' = 1$, j') states, even at $E_{coll} = 1.97$ eV, there is enough energy available to the reaction as the product internal energy is very low, and hence the reaction can go through multiple pathways.

B. Negative j'–θ correlation

It is well-established that for the title reaction, low impact parameter (total angular momenta) collisions correlate with backward scattering and vice versa. Furthermore, it has also been experimentally observed that, for a given v' manifold, the products became more backscattered with decreasing j'. This relation between product rotational excitation j' and scattering angle θ, better known as the negative j'–θ correlation, did not hold for the $v' = 4$ manifold at $E_{coll} = 1.97$ eV.[4,7] On the contrary, as j' increased, the products became more backscattered, as shown in Fig. 6. This anomalous behavior was explained by considering a centrifugal barrier in the exit channel of the $H + D_2 \rightarrow HD(v' = 4, j') + D$ reaction, the magnitude of which grows with increasing impact parameters.[4,7] At the $E_{coll} = 1.97$ eV, to form HD($v' = 4$, j') products, more than 85% of the total available energy is tied up in the internal energy of the products, leaving very little energy for the recoil. In the low recoil energy limit, the HD product molecule tends to be scattered with its internuclear axis parallel to the recoil direction, and the centrifugal barrier hinders the reaction except for small impact parameters. Hence, for $v' = 4$ at $E_{coll} = 1.97$ eV, larger j' correlates with smaller impact parameter which, in turn, involves more

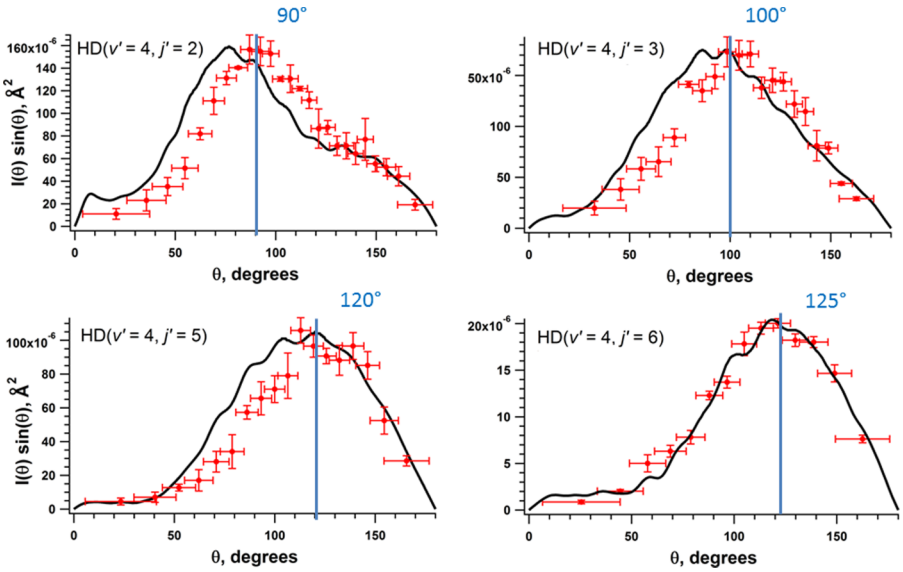

FIG. 6. The experimental (red dots) and theoretical (solid black curves) DCSs for the reaction $H+D_2 \rightarrow HD(v' = 4, j' = 2, 3, 5, 6)+D$ at the collision energy of 1.97 eV. The theoretical DCSs have been blurred to simulate the experimental conditions as described in the text. The error bars represent one standard deviation calculated from the statistical uncertainties in 5-10 different scans. The experimental peaks are designated by a solid blue line to show the anomalous behavior of the angular distribution, i.e., instead of showing the usual negative j'–θ correlation, the DCSs peak at higher values of theta as j' increases. These data have been previously reported in Ref. 7 and are shown here for the purpose of comparison with the data at $E_{coll} = 3.26$ eV.

backscattered products, which contradicts the well-established j'–θ trend.

The aforementioned arguments are supported by many theoretical results,[8] but no experiments were previously carried out to confirm their validity. Experimentally this can be shown in two ways: (i) this behavior should hold for any HD(v', j') state as long as the products are formed in the limit of low recoil energy; and (ii) if we measure the DCS of HD($v' = 4$, j') at energies high enough such that there is sufficient energy for the products to be formed from all possible impact parameters, we should observe the general negative j'–θ trend. In this study, we have undertaken the latter approach. The collision energy of the present work, $E_{coll} = 3.26$ eV, much higher than the previous collision energy of 1.97 eV, is well above the recoil limit of the products in $v' = 4$. Hence, it can be expected that the DCSs should show a negative j'–θ correlation; i.e., the products should become more forward scattered as j' increases. The peaks for DCSs of HD($v' = 4$, $j' = 6$, 8, 12) in Fig. 2 are marked by a solid orange line. As it can be observed, the most backscattered peak in the case of $j' = 6$ is at 120°; for $j' = 8$, it moves to 100°; moving further forward to 70° for $j' = 12$. Care should be exercised to extend this analysis to lower j' states, wherein the peaks of the DCSs are displaced by means of the quantum interferences between the *spiral* (direct recoil) and the *ear* mechanisms.[17]

IV. CONCLUSION

We have presented experimental and theoretical angular distributions for $H + D_2 \rightarrow HD(v' = 4, j') + D$ at a collision energy of 3.26 eV ($E_{tot} = 3.45$ eV), the highest energy at which reactive scattering has ever been measured for this reaction, well above the conical intersections which occur at $E_{tot} \cong 2.7$ eV. Our results show that the anomalous positive j'–θ trend observed for $v' = 4$ at $E_{coll} = 1.97$ eV no longer appears, thus confirming that it was a consequence of the very low recoil energy available for the $v' = 4$ manifold at 1.97 eV. In addition, we also have found that, as the total energy available increases, mechanisms other than direct recoil scattering (the *spiral*) start to participate and even dominate the scattering dynamics, giving rise to multiple peaks in the DCS through quantum interferences.

Applying the same QM and QCT analysis as that used for HD($v' = 1$, j') formation at 1.97 eV, we found that the backward/sideways scattered peaks in HD($v' = 4$, j') at 3.26 eV can be attributed to the presence of multiple mechanisms and the interference effects between them which were previously not seen at lower energies. This behavior leads us into recognizing another trend in this reaction, that is, for any given HD(v', j') product state, the mechanisms that will participate in its formation are highly dependent on the total energy available to the system, and as long as there are two or more mechanisms participating leading to product scattering in the same solid angle, there will be interference effects giving rise to oscillations in the DCSs. The presence of interference patterns in the angular distributions of reactive collisions is expected to be a general phenomenon, although their experimental detectability may be limited by a series of requirements: sufficiently narrow distribution of collision energies and initial rovibrational states, and to the right choice of a given final state with not too high rotational excitation.

At the collision energy of 3.26 eV, there are trajectories that surround the conical intersection and that would likely give rise to geometric phase effects. However, the good agreement between the results of QM calculations carried out without taking into account the geometric phase seems to indicate that this effect is not relevant, in particular, for the final rovibrational states explored in the present work as no trajectories surrounding the conical intersection were found for these states.

ACKNOWLEDGMENTS

The authors acknowledge funding by the Spanish Ministry of Science and Innovation (Grant Nos. CTQ2012-37404-C02, CTQ2015-65033-P, and Consolider Ingenio 2010

CSD2009-00038) and the US National Science Foundation (Grant Nos. CHE-1151428 and CHE-1464640).

[1]R. D. Levine, *Molecular Reaction Dynamics* (Cambridge University Press, Cambridge, UK, 2005).
[2]M. Brouard and C. Vallance, *Tutorials in Molecular Reaction Dynamics* (Royal Society of Chemistry, Cambridge, UK, 2010).
[3]F. J. Aoiz, L. Bañares, and V. J. Herrero, Int. Rev. Phys. Chem. **24**, 119–190 (2005).
[4]J. Jankunas, M. Sneha, R. N. Zare, F. Bouakline, S. C. Althorpe, D. Herráez-Aguilar, and F. J. Aoiz, Proc. Natl. Acad. Sci. U. S. A. **111**, 15–20 (2014).
[5]P. G. Jambrina, D. Herráez-Aguilar, F. J. Aoiz, M. Sneha, J. Jankunas, and R. N. Zare, Nat. Chem. **7**, 661 (2015).
[6]P. G. Jambrina, J. Aldegunde, F. J. Aoiz, M. Sneha, and R. N. Zare, Chem. Sci. **7**, 642 (2016).
[7]J. Jankunas, R. N. Zare, F. Bouakline, S. C. Althorpe, D. Herráez-Aguilar, and F. J. Aoiz, Science **336**, 1687–1690 (2012).
[8]J. Aldegunde, D. Herráez-Aguilar, P. G. Jambrina, F. J. Aoiz, J. Jankunas, and R. N. Zare, J. Phys. Chem. Lett. **3**, 2959–2963 (2012).
[9]N. E. Shafer, A. J. Orr-Ewing, W. R. Simpson, H. Xu, and R. N. Zare, Chem. Phys. Lett. **212**, 155–162 (1993).
[10]K. Koszinowski, N. T. Goldberg, A. E. Pomerantz, and R. N. Zare, J. Chem. Phys. **125**, 133503 (2006).
[11]H. Gao, M. Sneha, F. Bouakline, S. C. Althorpe, and R. N. Zare, J. Phys. Chem. A **119**, 12036 (2015).
[12]U. Fantz and D. Wünderlich, At. Data Nucl. Data Tables **92**, 853 (2006).
[13]A. I. Boothroyd, W. J. Keogh, P. G. Martin, and M. R. Peterson, J. Chem. Phys. **104**, 7139–7152 (1996).
[14]D. Skouteris, J. F. Castillo, and D. E. Manolopoulos, Comput. Phys. Commun. **133**, 128–135 (2000).
[15]F. J. Aoiz, V. J. Herrero, and V. Sáez-Rábanos, J. Chem. Phys. **97**, 7423–7436 (1992).
[16]J. Jankunas, M. Sneha, R. N. Zare, F. Bouakline, and S. C. Althorpe, J. Chem. Phys. **138**, 094310 (2013).
[17]S. J. Greaves, D. Murdock, E. Wrede, and S. C. Althorpe, J. Chem. Phys. **128**, 164306 (2008).
[18]S. C. Althorpe, F. Fernandez-Alonso, B. D. Bean, J. D. Ayers, A. E. Pomerantz, R. N. Zare, and E. Wrede, Nature **416**, 67–70 (2002).